# Theoretical Equilibrium Morphology of Gypsum (CaSO4·2H2O). 1. A Syncretic Strategy to Calculate the Morphology of Crystals

**ARTICLE** *in* CRYSTAL GROWTH & DESIGN · MAY 2010

Impact Factor: 4.89 · DOI: 10.1021/cg900660v



**3 AUTHORS:**

Francesco Roberto Massaro
University of Padova
**41** PUBLICATIONS **286** CITATIONS
SEE PROFILE

Marco Rubbo
Università degli Studi di Torino
**98** PUBLICATIONS **614** CITATIONS
SEE PROFILE

Dino Aquilano
Università degli Studi di Torino
**190** PUBLICATIONS **998** CITATIONS
SEE PROFILE

DOI: 10.1021/cg900660v

CRYSTAL GROWTH & DESIGN Article
2010, Vol. 10
2870–2878

# Theoretical Equilibrium Morphology of Gypsum ($CaSO_4 \cdot 2H_2O$). 1. A Syncretic Strategy to Calculate the Morphology of Crystals

Francesco Roberto Massaro,*,† Marco Rubbo,‡ and Dino Aquilano‡

†*Dipartimento di Scienza dei Materiali – Università di Milano Bicocca, via R. Cozzi 53, I-20125 Milano, Italy, and* ‡*Dipartimento di Scienze Mineralogiche e Petrologiche – Università di Torino, via Valperga Caluso 35, I-10125 Torino, Italy*

*Received June 12, 2009; Revised Manuscript Received March 9, 2010*

**ABSTRACT:** The theoretical and equilibrium morphology of gypsum ($CaSO_4 \cdot 2H_2O$) is reassessed, starting from the historical papers by Simon and Bienfait (1965) and by Heijnen and Hartman (1991). The surface profiles of the most frequently observed crystal forms have been determined following two ways: in the first one we used the Hartman–Perdok method based on the periodic bond chain (PBC) analysis, while in the second one the profile of each face was obtained using the GDIS program. In both cases, the calculation of the specific surface energy values has been made using the general utility lattice program (GULP) code. From the synthesis of the two methods, a new and much more isotropic equilibrium shape is calculated, in the case of both unrelaxed and relaxed surfaces. Further, and for the first time, beyond the well-known and singular {010}, {120}, {0$\bar{1}$1}, and {$\bar{1}$11} F-forms, two stepped, {100} and {$\bar{1}$22}, and one kinked form, {$\bar{1}$02}, are found to build the equilibrium shape of gypsum.

## 1. Introduction

Investigations on the kinetics of nucleation and growth, and on the morphology of single and twinned crystals of gypsum ($CaSO_4 \cdot 2H_2O$) have been developed for a long time, owing to the interest in this widespread mineral both from a geological and an industrial point of view. In these kinds of studies, it is of prime importance to obtain all the surface properties of the crystal on a theoretical ground, particularly as gypsum usually crystallizes from solutions in a wide range of compositions, according to whether the crystallization takes place in a natural, laboratory, or industrial environment. In other words, the master problem to face is to determine the relative weight of the static surface energy over the kinetic factors in determining the gypsum habit. Among the kinetic factors again we include the attachment energies usually considered an estimate of the affinity of crystallization over the different faces and processes at the atomic level as, for example, desolvation of surface sites. To tackle the problem, the first step is the calculation of the theoretical equilibrium morphology in the absence of water and the successive one is to determine how this shape can be modified by the adsorption either of water or of other solution components. This way of working should be also extended to the two-dimensional (2D) nuclei that can form on the flat crystal faces in order to assess the step free energies (without and with water adsorption) and, consequently, to determine their shapes at equilibrium.

A few sound papers have been devoted to interpret the morphology of gypsum in terms of the crystal structure. The pioneering work was performed by Simon[1] and Simon and Bienfait[2] who carried out a periodic bond chain (PBC) analysis and calculated both the theoretical equilibrium (E.S.) and growth (G.S.) shapes of the crystal considering Coulomb interactions based on a specific charge distribution (Ca = $+2e$, S = $+0.3e$, O($SO_4^{2-}$) = $-0.575e$, H = $+0.326e$, O($H_2O$) = $-0.652e$). Further, an accurate determination was performed of the stability of the monolayered steps building the 2D nuclei on all the flat (F) forms, that is, {010}, {120}, {011} and {$\bar{1}$11}. Here and in the following, the forms are indexed according to de Jong and Bouman[3] who chose a lattice frame related to the gypsum morphology.

Much later, Weijnen et al.[4] investigating the adsorption of additives at the gypsum crystal surfaces were the first to consider how slices $^1/_2 d_{hkl}$ thick can exist on both {011} and {$\bar{1}$11} forms, as theoretically suggested by Hartman and Heijnen.[5] To calculate the interaction energies (by a broken bond model) the charge on the sulfur atom and on each oxygen atom in the sulfate ion were assumed to be $+1.34e$ and $-0.84e$, respectively, as calculated by Gelius et al.[6] in a MO-SCF-LCAO study. The charges on the oxygen and on the hydrogen of water, amounting respectively to $-0.702e$ and $+0.351e$ were those by Del Re.[7]

A more complete investigation on the relationships between structure and morphology of gypsum is given in the paper by Heijnen and Hartman[8] who found that {$\bar{1}$22} is another F form and calculated both the equilibrium and growth shapes. They used an electrostatic point charge model and considered several different charge distributions on the atoms of water and on the sulfate. The theoretical habits they obtained are tabular {010} and show the forms {120}, {011}, and {$\bar{1}$11}, listed in order of decreasing morphological importance. Further, they found that both the {011} and {$\bar{1}$11} forms "...can grow by slices of thickness $^1/_2 d_{011}$ and $^1/_2 d_{\bar{1}11}$ and that the difference in attachment energy of the two occurring slices {011} is smaller than for {$\bar{1}$11}. Therefore, the (011) face can start growing by half slices at lower supersaturations than ($\bar{1}$11); consequently, the (011) face grows faster and then ($\bar{1}$11) becomes the larger terminating face..." Hence, they removed the discrepancy between theory and observation, in good agreement with the fact that {$\bar{1}$11} usually dominates on the{011} form, both in natural and laboratory crystals.

The solvent interaction was the key to give a qualitative explanation for other discrepancies between the theoretical and observed habits of gypsum. Van der Voort and Hartman[9] imagined that two kinds of water molecules can be present on the crystal faces. One kind of water belongs to the crystal structure and is not removed when the face advances: this is

*Corresponding author. E-mail: dino.aquilano@unito.it. Tel: +39 011 6705125. Fax: +39 011 6705128.

 Published on Web 05/18/2010 

the case of the {011} form. The other kind does not belong to the crystal structure and then must be desorbed before the face can continue growing: thereby the advancement rate of the face is lowered: it is the case of the $\{\bar{1}11\}$ form.

In all research we mentioned, attention has been focused on the $\{hkl\}$ forms having F character, this reductive view being legitimated by the prevailing occurrence of the flat forms on theoretical equilibrium and growth shapes of crystals. However, it is well-known that stepped (S) and kinked (K) forms can enter the growth morphology of crystals, owing to the temporary solvent and/or impurity adsorption which can change the character of unstable forms (S, K) to the stable one (F), through the generation of new periodic bond chains (PBCs) in the outmost growing surfaces.[10] It is also worth remembering that theoretical calculations on specific surface energy ($\gamma_{hkl}$) are usually carried out on unrelaxed surfaces. However, this quantity is strongly anisotropic and relaxation cannot be neglected especially when alternative ways of reconstruction of polar surfaces can be envisaged. This is the case, for instance, of the equilibrium shape of calcite ($CaCO_3$) calculated with respect to a vacuum. As a matter of fact, this E.S. has been always retained built only by the $\{10\bar{1}4\}$ cleavage rhombohedron, while is actually made as well by the acute $\{01\bar{1}2\}$ rhombohedron and the {0001} pinacoid[11] when the surface relaxation is taken into account. These new and highly recurrent forms have F and K character, respectively.

In the case of gypsum, we know from the literature[3,12] that the stepped forms {100}, {001}, $\{10\bar{1}\}$, and $\{\bar{1}02\}$ belong to its morphology and, it has been very recently found,[13] that the vicinal {140} and {160} forms dominate the [001] zone when growth occurs in a natural environment, at very low supersaturation and at a temperature ranging between 55 and 58 °C.

On the ground of these considerations, we planned to revisit the prediction of both equilibrium and growth morphology of gypsum. The work will follow two ways:

(i) In the first one, the Hartman−Perdok method[14] will be applied as a guide to find the optimal profile of every face and among alternative profiles, if any, for the same $\{hkl\}$ form,

(ii) In the second one, the profile of each face will be obtained using the GDIS program.[15]

Then a synthesis will be made; in both cases, the energy calculations will be made using the GULP code.[16]

When predicting both equilibrium and growth morphology of crystals, the usually employed strategies do not take into account the constraints inherent in the Hartman−Perdok method for evaluating the character of the crystallographic $\{hkl\}$ forms along with their most probable surface profiles. As a consequence, the space of the configurations of a crystal face is only partially explored. The surface representing the surface free energy at 0 K exhibits many local minima. In a static energy minimization, the local minimum is accessed closest to the initial configuration of the crystal face. So, it is important to span the whole space of the configurations of a given crystal surface: these can be calculated for a crystal in a vacuum, complying with the constraints exposed in the following sections. An incorrect determination of the surface profile generates incorrect equilibrium and growth shapes. As the behavior (reactivity, epitaxy, adsorption, etc.) of a crystal face is strictly related to its configuration and stability, we propose a rigorous method for surface profile prediction. This is the sense of comparing and integrating the Hartman−Perdok method and GDIS way of calculating all possible surface profiles for all potential crystal faces.

In this work, our attention will be confined to the following forms: {010}, {120}, {011}, $\{\bar{1}11\}$, $\{\bar{1}22\}$, {100}, {001}, and $\{\bar{1}02\}$. In a forthcoming paper, we will deal with the stability of the vicinal faces and mainly of those developing in the [001] zone; peculiar care also will be paid to the understanding of the growth aspects of the contact {100} twin law. Further, all the calculations will be done on both unrelaxed and relaxed surfaces with respect to a vacuum, at room temperature.

As mentioned above, we adopt throughout this paper the morphological reference frame of de Jong and Bouman,[3] for the reasons explained by Heijnen and Hartman.[8] Thus, the $z$ axis coincides with the needle axis along which the gypsum plates spontaneously develop and the $x$ axis forms an angle of near 114° with it. In Appendix I, the geometrical and structural relationships between this choice and the alternative ones that can be found in the literature are given.

Finally, at variance with this work, the force fields assumed in the previous works were very simple and not parametrized on the crystal properties.

## 2. Energy Calculations and Construction of the Surfaces

Atomistic modeling is based on the Born model, and the long- and short-range interactions are described by simple analytical functions. The model we adopt has been worked out by Adam[17] who used both transferable potentials from the literature and devised potentials for the interaction of the water molecule with calcium and sulfate ions. Adam optimized the parameters of the potential functions describing the interactions between $Ca^{2+}$ and $SO_4^{2-}$ with water, fitting to the crystal structure by Pedersen[18] elastic constants and selected IR frequencies for gypsum. The fitting procedure is implemented in the general utility lattice program (GULP).[16] The model is a quite sophisticated one, taking into account intramolecular and interatomic interactions, the three-body force within the $SO_4^{2-}$ ions, and the polarization of the oxygen atom in the water (w) molecule by the shell model in which the ions are made by a massive positive core coupled to a mass-less negative shell (s) by a harmonic spring potential; the net ionic charge is fixed.

In summary, we use the following semiempirical potential functions:

(i) the Buckingham potential to represent the interaction between atoms $i$ and $j$:

$$U_{ij}(r) = A_{ij} \times \exp(-r/\rho_{ij}) - C_{ij} \times r^{-6}$$

where $ij$ stand for Ca−O, Ca−$O_{ws}$, O−$O_{ws}$, H−O, O−O, H−$O_{ws}$;

(ii) the Morse potential modeling the intra-atomic interactions within ionic groups:

$$U_{ij}(r) = D_{ij} \times \{[1 - \exp[-\beta_{ij}(r - r_{0,ij})]]^2 - 1\}$$

where $ij$ stand for O−S, H−$O_{ws}$;

(iii) the Lennard-Jones 6-12 potential to model the interactions between the oxygen atoms of the water molecules

$$U_{ij}(r) = A_{ij}r^{-12} - B_{ij}r^{-6}$$

where $ij$ stand for: $O_{ws}$−$O_{ws}$;

(iv) the three-body force within the ions $SO_4^{2-}$ and within the water molecules:

$$U_{ij}(r) = \frac{1}{2}k_\theta(\theta - \theta_0)^2$$

where $ij$ stand for O−S−O, H−$O_w$−H;

(v) the shell model potential to represent the polarization of the oxygen atoms of the water molecules:

$$U_{ij}(r) = \frac{1}{2}k_s(r - r_0)^2$$

where *ij* stand for $O_{wc}-O_{ws}$. The numerical values of the constants occurring in the different potential functions are drawn in Appendix II.

To complete the description of the model, we give the numerical values of the parameters and refer to the paper by Adam[17] where the interested reader can find the bibliographic sources of the potential energy functions and a discussion on the quality of the model and on its ability to fit the observed properties of gypsum.

Finally long-range electrostatic interactions are generated by the following set of charges:

$$\text{Ca: } +2.00e, \text{S: } +1.36e, \text{O: } -0.84e,$$
$$O_w\text{core: } +1.00e, O_w\text{ shell: } -1.82e, \text{H: } +0.41e$$

In order to identify the PBCs, we qualitatively evaluated the bond strength on the ground of bond distances, in particular considering also the hydrogen bonds geometry. However, we did not calculate the energy of the interactions O−H−O following the Adam's model as, at the level of PBC identification, it is not necessary.

The construction of the surfaces and their structural manipulation to build layers following the Hartman method is performed by graphical means, independently of the program for energy calculations. This is achieved by the GDIS[19] program (http://gdis.seul.org/) developed by Fleming and Rohl.[15] Using GDIS, one can cut a crystal into two regions separated by a plane *hkl*. Region 2 has such a thickness to represent the bulk, while the thickness of region 1 should ensure convergence of the surface energy. In our calculation, the two regions have the same thickness and convergence has been assessed for every plane and shift.

As a rule, several symmetry different cuts are possible at different distances or shifts *s* from a reference point such that $0 < s \leq d_{hkl}$. Valid shifts satisfy the following constraints:

(i) Strongest bonds, for example, bonds within ionic groups as $SO_4^{2-}$, are not cut;
(ii) Within the regions the stoichiometric ratios are observed;
(iii) The regions are electrically neutral and cannot have a macroscopic dipole moment.

The different surfaces so generated exhibit different groups of atoms. Reasoning in terms of the periodic bonds model, the uppermost $d_{hkl}$ layer can contain complete PBCs or partial PBCs made by one or more primitive PBCs[20] and additional ions or molecules.[21,22] As a consequence, the ensemble of configurations of the layers $d_{hkl}$ thick, obtained by the shifts, intersects the less numerous ensemble obtained by looking for the strongest complete PBCs identified by the Hartman−Perdok analysis. The overlap may be partial because the Hartman−Perdok analysis is usually limited to the first coordination sphere, and conversely, it may occur that some complete PBCs are not generated by the allowed shifts. In the latter cases, the surface profile obtained by the appropriate shift is remodeled removing from the upper layer the units exceeding the complete PBCs and translating them into an equivalent position at the bottom of region 1.

The equilibrium morphology of gypsum is obtained from the minimal surface athermal energy, at constant volume, sorted out by combining the energies associated with the surface profiles generated by the two methods.

In the following sections, the results will be exposed on the calculation of the athermal surface energy at constant volume. In this condition, for every {*hkl*} form, the surface configuration stable at 0 K is overwhelmingly dominant at high temperature. However, on the basis of previous studies,[23,24] we expect that thermal and configurational contributions can slightly smooth the differences between the surface free energies of different configurations of the same form. Moreover, when the system consists of the crystal and of an aqueous solution, which is the interesting situation dealing with gypsum, the chemical potential of components in solution may favor one among the possible profiles a (*hkl*) face can show, depending on binding sites for adsorption and surface reactions occurring. For these reasons, we are interested to find out at least the set of most likely surface configurations of all faces, including those having S and K character. Indeed, as it will be seen, the latter have a high degree of freedom to reconstruct themselves producing, let say, "surface periodic chains" within the uppermost layer.

## 3. Characters and Surface Profiles of the {*hkl*} Forms of Gypsum

We partially confirm the results obtained by Simon and Bienfait[2] and improved by Heijnen and Hartman[8] on the character of the crystallographic forms of gypsum. As a matter of fact, by rigorously applying the Hartman−Perdok analysis, we assessed that the end chain energy (ECE)[2] of the [001], [100], [0$\bar{1}$1], and [211] chains is negative, so they are indeed PBCs, and we found that {010}, {120}, {011}, {$\bar{1}$11} forms show F character, while {$\bar{1}$22}, {100}, and {001} are stepped and {$\bar{1}$02} is a kinked form.

In Table 1 these results are expressed quantitatively; the forms are ranked according to their specific athermal surface energies obtained by applying both the shifts method and the one based on the PBCs. It can be seen that the surface profile of the forms {120}, {011}, {100} cannot be obtained only by the shifts calculated by GDIS and that one profile of the {011} produced by the PBC analysis has the lowest energy value. Conversely, the lowest surface energy of the {120}, {100}, and {$\bar{1}$11} forms are associated with profiles obtained by GDIS. When the facing profiles of the two regions separated by a *hkl* plane have complementary configuration, the (*hkl*) face exhibits two surface profiles $(hkl)_\alpha$ and $(hkl)_\beta$: then, $(hkl)_\alpha$ and $(hkl)_\beta$ relax in a different way and have different surface energies. These cases are indicated in the table by two arrows relating the unrelaxed to the relaxed values of the surface energies. In an experiment, we measure the free energy of formation of the two surfaces but only by a model we can assign the different values of the relaxation energies.

We discuss now in detail the surface profiles, according to their zone axes.

**3.1. [001]: The Main Zone Axis of the Gypsum Crystal.** The crystal structure of gypsum, projected along this zone axis, is drawn in Figure 1. An enlarged view of the PBC $[001]_a$ is represented in the center of Figure 1a, along with its periodic development (Figure 1b). The distribution of bonds within this PBC is such that dipole moments are symmetry related with respect to the chain axis and then the slices of thickness $d_{020}$ and $d_{120}$, both built by parallel sequences of PBCs $[001]_a$, are terminated by nonpolar surface profiles.

As found by Simon and Bienfait,[2] the [100] and [211] PBCs connect the $[001]_a$ PBCs within the $d_{020}$ and $d_{120}$ slices, giving

**Table 1. The Specific Surface Energies $\gamma$ (erg cm$^{-2}$) of Each {*hkl*} Form of Gypsum Are Reported on Horizontal Strips**[a]

| Form {hkl} | Growth mode | $U_{PBC}$ unrelaxed | $R_{PBC}$ relaxed | $\Delta_{UR}$ (%) | $U_{SCM}$ unrelaxed | $R_{SCM}$ relaxed | $\Delta_{UR}$ (%) |
|---|---|---|---|---|---|---|---|
| {010} | F | (a) 463 | 432 | -6.69 | 463 | 432 | -6.69 |
| | | | | | 796 | 503 | -36.80 |
| | | (b) 1123 | 965 | -14.07 | | 752 | -5.52 |
| | | | | | 1123 | 965 | -14.07 |
| {120} | F | (a) 735 | 561 | -23.67 | 712 | 543 | -23.73 |
| | | | | | | 579 | -18.68 |
| | | (b) 763 | 621 | -18.61 | 763 | 621 | -18.61 |
| | | | | | 822 | 561 | -31.75 |
| | | | | | | 694 | -15.57 |
| | | | | | 888 | 702 | -26.49 |
| {011} | F | (a) 1021 | 757 | -25.85 | | | |
| | | (b) 1052 | 773 | -26.52 | 1052 | 773 | -26.52 |
| | | (c) 1136 | 768 | -32.39 | 1136 | 768 | -32.39 |
| {$\bar{1}$11} | F | (a) 1318 | 840 | -36.26 | 1318 | 840 | -36.26 |
| | | (b) 1428 | 1027 | -28.08 | 1428 | 1027 | -28.08 |
| | | | | | 1517 | 795 | -47.59 |
| | | | | | | 971 | -35.99 |
| {$\bar{1}$22} | S | 1312 | 781 | -40.47 | 1312 | 781 | -40.47 |
| | | | | | 1441 | 793 | -44.97 |
| | | | | | | 895 | -37.89 |
| | | | | | 1969 | 844 | -57.13 |
| | | | | | | 917 | -54.87 |
| | | | | | 2139 | 878 | -58.95 |
| {100} | S | (a) 865 | 678 | -21.62 | 837 | 616 | -26.40 |
| | | | | | | 713 | -14.81 |
| | | (b) 886 | 706 | -20.31 | 886 | 706 | -20.31 |
| {001} | S | 1642 | 981 | -40.25 | 1617 | 825 | -48.98 |
| | | | | | | 1048 | -35.19 |
| | | | | | 1642 | 981 | -40.25 |
| {$\bar{1}$02} | K | 1334 | 982 | -26.38 | 1334 | 982 | -26.38 |
| | | | | | 1465 | 972 | -33.65 |
| | | | | | | 991 | -32.35 |

[a] The values are obtained by determining the surface profiles either through the PBC method or by the systematic surface cuts (SCM). The letters (a,b,c) in the $U_{PBC}$ *unrelaxed* column refer to different surface profiles obtained through different PBCs developing along the same direction (see text). The difference between unrelaxed and relaxed profiles are also indicated ($\Delta_{UR}$ (%)). The arrows indicate the splitting of the surface energy when the cut generates two unrelaxed profiles not symmetry related.

rise to the $\{010\}_a$ and $\{120\}_a$ F-forms, respectively. The corresponding profiles originate the specific surface energy values $\gamma^{U}_{010(a)} = 463$ erg cm$^{-2}$ and $\gamma^{U}_{120(a)} = 735$ erg cm$^{-2}$ for the unrelaxed surfaces.

From Table 1 one can see that the surface relaxation plays a minor role on the {010} surfaces compared to the {120} ones, as it ensues from the structure of the $d_{020}$ slice which is not only the most compact one in the whole crystal but also determines the only perfect surface of cleavage.

The different behavior of the {010} and {120} surfaces with respect to the relaxation is a good example to explain the very reason why the method we applied is more advanced with respect to the past methods and to the current way of cutting the surfaces as they might be confused with ideal planes. In fact:

(a) From the rigorous constraints inherent to the PBC method, both the $[001]_a$ and $[001]_b$ PBC are generated, the $[001]_a$ PBC being the strongest between the two allowed [001] PBCs. Consequently, from the $(010)_a$

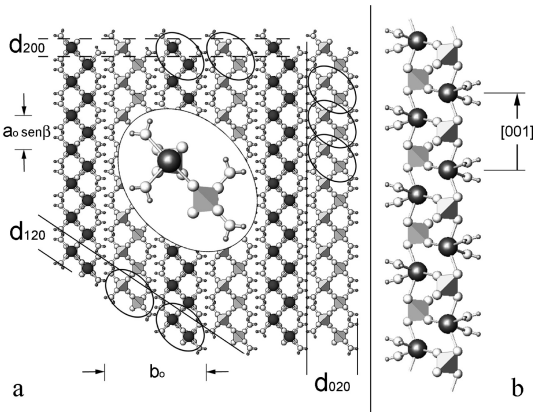


**Figure 1.** (a) Gypsum structure projected along the [001] direction. The $[001]_a$ PBC allows one to draw the surface profiles of the $\{010\}_a$ and $\{120\}_a$ F-forms and of the $\{100\}_a$ S-form. (b) The development of the $[001]_a$ PBC showing the strong Ca−O($SO_4^{2-}$) bonds between the polar [001] chains.

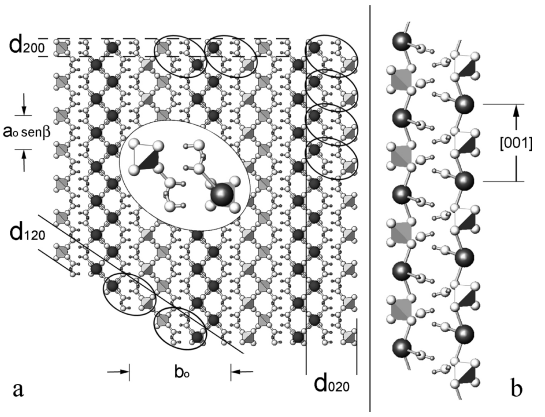


**Figure 2.** (a) Gypsum structure projected along the [001] direction. The $[001]_b$ PBC allows one to draw the surface profiles of the $\{010\}_b$ and $\{120\}_b$ F-forms and of the $\{100\}_b$ S-form. (b) The development of the $[001]_b$ PBC showing the hydrogen bonds ($O_w$−H···O($SO_4^{2-}$)) between the polar [001] chains.

and $(120)_a$ profiles (that can be obtained from this PBC) the lowest surface energy values are derived: 463 and 735 erg $cm^{-2}$ for $\gamma_{(010)a}$ and $\gamma_{(120)a}$, respectively.

(b) When relaxation is considered, one can see that the $(120)_a$ profile is much more affected than the $(010)_a$ one, as it follows from the reduction factors: $[\gamma_{(120)a}^{relax} - \gamma_{(120)a}^{unrelaxed}]/\gamma_{(120)a}^{unrelaxed} = -23.67\%$ and $[\gamma_{(010)a}^{relax} - \gamma_{(010)a}^{unrelaxed}]/\gamma_{(010)a}^{unrelaxed} = -6.69\%$.

This is not surprising if one just compares the orientation of the two water molecules (per formula unit) in the respective layers. Within a $d_{020}$ layer both molecules must maintain dipole components perpendicular to the surface plane, owing to the symmetry $A_2$ axis (which is normal to the 010 symmetry plane) that continues working, before and after relaxation. This no longer holds for the $d_{120}$ layer, since the two water molecules (which are obviously related by symmetry $A_2$ axis in the bulk of the crystal) can relax without symmetry constraints, since no symmetry element exists normal to the 120 plane. A similar reasoning applies when comparing the two less probable $(010)_b$ and $(010)_b$ interfaces exhibiting the Ca and the $SO_4$ growth units in contact with the mother phase. This is the very structural reason for explaining the different behaviors of the two surfaces from the relaxation point of view.

Concerning the consequences of this striking difference in the equilibrium shape of the crystal, it is worth considering as an example that [001], the most important zone in determining the averaged value of the surface energy for gypsum, is deeply modified when going from the Simon−Bienfait (unrelaxed) values to those (relaxed) obtained in the present work. As a matter of fact, let us compare $\gamma_{(010)Simon} = 170$ erg $cm^{-2}$ and $\gamma_{(120)Simon} = 440$ erg $cm^{-2}$ with the corresponding values we obtained ($\gamma_{(010)} = 432$ erg $cm^{-2}$ and $\gamma_{(120)} = 561$ erg $cm^{-2}$): the equilibrium shape of gypsum dramatically changes, as one will see in Figures 8 and 9. Further, when drawing the equilibrium shape of the crystal in the [001] zone, the resulting weighted value of the surface energy varies from $<\gamma>_{Simon} = 260$ erg $cm^{-2}$ to $<\gamma>_{this\ work} = 507$ erg $cm^{-2}$. From the comparison between these two values, one can imagine the dramatic consequences on the 3D - nucleation frequency ($J_{3D}$) of gypsum, having kept in mind that $J_{3D} \approx \exp\{[-f\Omega^2\langle\gamma\rangle^3]/[(kT)^3(\ln\beta)^2]\}$, where $f$ is a numerical shape factor, $\Omega$ is the molecular volume in the crystal, $k$ is the Boltzmann constant, $T$ is the absolute temperature, and $\beta$ is the relative supersaturation value in solution.

Besides the two above-mentioned F forms, there is another form in the [001] zone, the {100} S-form, which is definitely important when dealing with the most frequently occurring twin law of gypsum. The importance of this form has been overlooked up to now, probably because of its stepped character, whereas it should be competitive in the nucleation morphology thanks to its fairly low $\gamma$ values. Here we will not deal with the growth aspects of the (100) twin law of gypsum, but confine our attention to the relevant fact that the {100} S-form can enter the equilibrium shape of the gypsum crystal, as it comes out from the values quoted in Table 1 and from the drawings shown in Figure 9.

Beyond the $[001]_a$ PBC, another periodic bond chain, the $[001]_b$ PBC can be found parallel to the $z$ axis, as shown in Figure 2b. By means of this alternative PBC, which also fulfills the condition of no dipole moment perpendicular to the [001] direction, the new profiles $\{010\}_b$, $\{120\}_b$, and $\{100\}_b$ are obtained, as illustrated in Figure 2a.

An emblematic case is one profile of the {010} form calculated by the GDIS shifts: in this case a third interface, $\{010\}_c$, can be obtained cutting the strong bonds between the $Ca^{2+}$ ions and the oxygen atoms of water molecules (Figure 3a): in this way, all the water molecules belonging to the $d_{020}$ slice lie on one side of the wavy interface while calcium and sulfate ions lie on the other side. Thus, the interface is situated neither on the symmetry centers nor on the glide planes: this represents the profound difference with the PBCs method. The calculation of the $\gamma$ value for this asymmetric slice is not affected by convergence problems since the dipole moment for both sides of the slice is canceled out either by the glide plane (for the $Ca^{2+}$ and $SO_4^{2-}$ ions) or by the symmetry centers (for water molecules), as outlined in Figure 3.

The energy value of the unrelaxed surfaces is 796 erg $cm^{-2}$. It is also plain that the surfaces of the two half crystals, being not symmetry related, split into two different relaxed surfaces: the $\gamma_{010(w)}$ value of the "hydrated" one is 503 erg $cm^{-2}$ while that of the complementary surface is 752 erg $cm^{-2}$. These values are comprised in between those calculated by the PBC method.

It can be useful to remember that the hydrated (010) surface was already studied by van der Voort and Hartman[9]

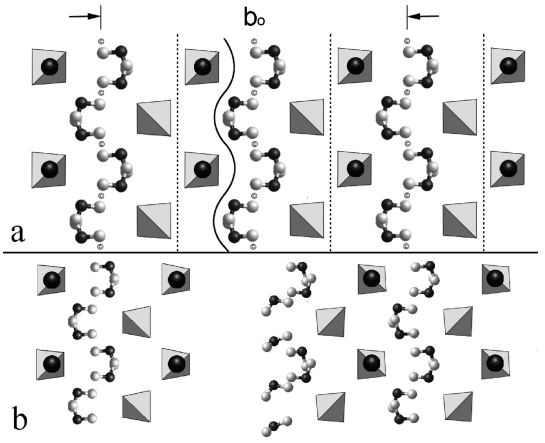


**Figure 3.** Gypsum structure projected along the [001] direction. (a) The wavy $\{010\}_c$ interface drawn in the bulk structure represents the third choice, beyond the $\{010\}_a$ and $\{010\}_b$ interfaces, for the {010} form. One can easily see that the interface lies neither on the symmetry centers (in between water molecules) nor on the glide planes (in between sulfate and calcium ions). (b) The two separated surface profiles, generated by the splitting of the $\{010\}_c$ interface, after surface relaxation.

when dealing with the attachment energies and the theoretical habit of gypsum growing from pure aqueous solution.

A similar analysis has been carried out for the crystal forms reported in Table 1. It can be seen that relaxed surfaces produced by symmetry breaking cuts can have the lower energy, in some cases. The discussion of this fact will be presented in a future work.

Now, we will deal with the probability for the different surfaces to occur in the equilibrium shape of the crystal. According to Hartman and Heijnen,[5] when a $\{hkl\}$ form has more than one-slice configuration, the stability of the $i$th slice is measured by the probability ($x_i$) of its occurrence in the equilibrium form. From the Boltzmann distribution:

$$x_i = \frac{\exp(-E_{s(i)}/RT)}{\sum_1^n \exp(-E_{s(i)}/RT)} \quad (1)$$

$$\text{where } E_{s(i)} = [(2V \times N_A)/(z \times d_{hkl})]\gamma_{hkl}^{(i)} \quad (2)$$

is the interfacial energy (per mole) of the $i$th slice configuration calculated in a vacuum ($V$, $z$, and $N_A$ being the volume of the elementary cell, the number of formula units in the elementary cell and the Avogadro's number, respectively), the sum being carried out over all the $n$ possible configurations. The sum is limited to the more stable configurations, the weight of the remaining being negligible.

In eq 2 we can safely use our $\gamma_{hkl}^{(i)}$ values calculated at 0 K. The $\gamma_{hkl}^{(i)}$ values although calculated at 0 K can give a good estimate of the probability $x_i$ as the weight of entropy is a few percent of the separation work at low temperature.

Let us consider, as an example, the set of forms belonging to [001], the most important zone axis of the crystal. When introducing in relation 1 all the $\gamma_{hk0}$ values quoted in Table 1 of the {010}, {120}, and {100} forms, it ensues that the only stable surfaces, in the [001] zone, are those corresponding to the $\{010\}_a$, $\{120\}_a$, and $\{100\}_a$ profiles. At first sight, this number of stable profiles might look too limited. Actually, some alternatives profiles excluded at very low temperature might contribute to the equilibrium shape of the crystal, when entropic terms (configurational and vibrational) are considered at higher temperature. A second more important factor is the water adsorption. In fact, it was recently proved[25] that the cooperative effect of temperature and solvent adsorption strongly reduces both the absolute values and the differences among the $E_{s(i)}$ values related to the different profiles belonging to the same $\{hkl\}$ form.

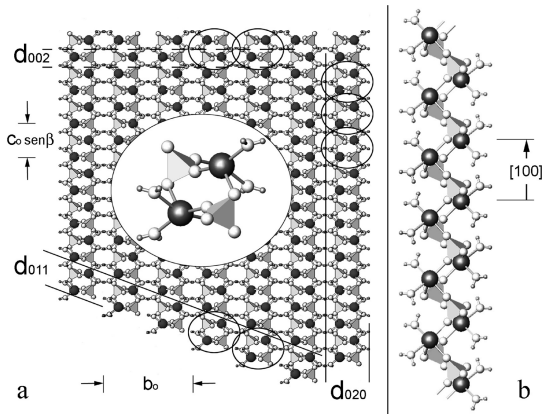


**Figure 4.** (a) Gypsum structure projected along the [100] direction. The $[100]_a$ PBC allows one to draw the surface profiles of the $\{010\}_a$ and $\{011\}_a$ F-forms and of the {001} S-form. (b) The development of the $[100]_a$ PBC showing the strong Ca−O($SO_4^{2-}$) bonds between the polar [100] chains.

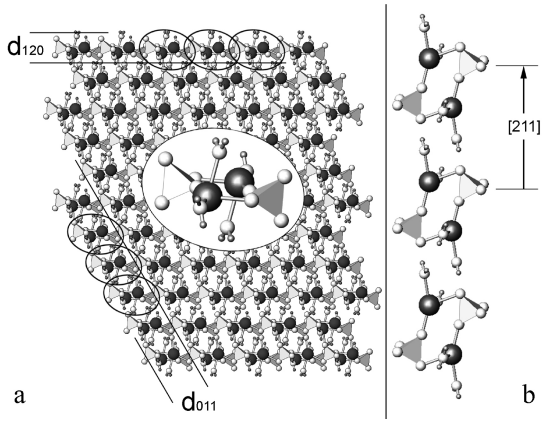


**Figure 5.** (a) Gypsum structure projected along the [211] direction. From the [211] PBC are obtained the surface profiles of the $\{120\}_a$ and $\{011\}_b$ F-forms. (b) The development of the [211] PBC showing the strong Ca−O($SO_4^{2-}$) bonds between the polar [211] chains, built by alternating Ca−O($SO_4^{2-}$) and $O_w$−H···O($SO_4^{2-}$) bonds.

**3.2. The [100], [211], and [0$\bar{1}$1] zones.** The projection of the gypsum structure along the [100] direction is drawn in Figure 4a, while the development of the $[100]_a$ PBC is represented in Figure 4b. The $[100]_a$ PBCs are connected within a $d_{020}$ slice through the above-mentioned $[001]_a$ PBCs and confirms the F character of the {010} form.

Within the slice of thickness $d_{011}$ the $[100]_a$ PBCs are linked along the $[0\bar{1}1]$ and $[2\bar{1}1]$ directions corresponding to the PBC of type $\langle 011\rangle$ and $\langle 211\rangle$, respectively. This means that the {011} prism has a strong F character because it contains three kinds of PBC in the thickness $d_{011}$ allowed by the extinction rules. Further, one can see that this form can exhibit three different profiles; two out of them $\{011\}_a$ and $\{011\}_b$ are obtained from the $[100]_a$ and [211] PBCs, respectively, as shown in Figures 4a and 5a. The third one, $\{011\}_c$, obtained from the PBCs $[100]_b$ (not shown), is described in Figure 6, where all the {011} profiles are compared.

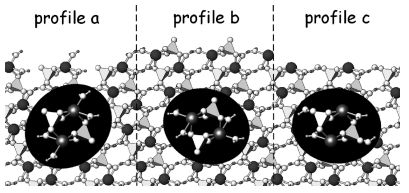


**Figure 6.** Detailed view of the three unrelaxed surface profiles that can be obtained through the PBC analysis. Each type of [100] PBC is represented in the three enlarged views and is rigorously contained within a slice of thickness $d_{011}$. When considering Table 1, it is worth outlining that the minimum energy profile $(011)_a$ which corresponds, after relaxation, to $\gamma_{(011)a}$=757 erg cm$^{-2}$, cannot be obtained through the systematic cuts, since the ideal 011 scanning plane "eliminates" the outermost water molecules.

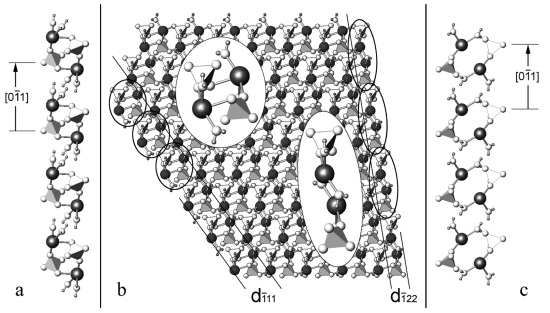


**Figure 7.** Projection along the [0$\bar{1}$1] direction of the gypsum structure: (a) Development of the PBC $[0\bar{1}1]_a$, corresponding to the enlarged view on the left side of Figure 7b. (b) From this PBC the $\{\bar{1}11\}_a$ surface profile originates, the $Ca^{2+}$ ions lying on the borders of the corresponding slice. The enlarged view of the PBC $[0\bar{1}1]_b$ is drawn on the right side of the figure, along with the slice associated to the $\{\bar{1}22\}$ form. (c) Development of the PBC $[0\bar{1}1]_b$.

The analysis of Figure 4a shows also the stepped character of the {001} form, owing to the fact that the $d_{002}$ thickness, allowed by the extinction rules, contains only one-half of the entire $[100]_a$ PBC. However, in spite of its character, the {001} pinacoid shows moderate surface energy values thanks to the strong relaxation undergone by its different surface profiles.

To complete the picture of the F faces, one has to consider the $\langle 0\bar{1}1\rangle$ PBCs represented in Figure 7:

(a) From the projection along the [0$\bar{1}$1] direction one can see the $[0\bar{1}1]_a$ PBCs (Figure 7a and enlarged view on the left side of Figure 7b). These PBCs are linked, within a slice of thickness $d_{\bar{1}11}$ through the [211] PBC: hence, the $\{\bar{1}11\}$ form assumes a flat character. The $\{\bar{1}11\}_a$ surface profile drawn in Figure 7b corresponds to the PBCs $[0\bar{1}1]_a$ and contains the $SO_4^{2-}$ groups in the middle of the $d_{\bar{1}11}$ slice.

An alternative profile $\{\bar{1}11\}_b$ (not drawn) can be obtained by a parallel shift of the slice of 1/2 $d_{\bar{1}11}$: in this case the $Ca^{2+}$ ions will lie in the midslice. The corresponding relaxed values of the surface energy are 840 and 1027 erg cm$^{-2}$, respectively. An allowed shift divides the crystal in two regions separated by a mean $\bar{1}11$ plane and the two parts are not related by the symmetry center; this implies that, for a unique value of the surface energy of the unrelaxed interface, two different values (795 and 971 erg cm$^{-2}$) are obtained for the corresponding relaxed surfaces. According to Hartman and Heijnen,[5,8] the existence of the two alternative profiles $\{\bar{1}11\}_a$ and $\{\bar{1}11\}_b$, along with their almost equal surface energy values, allows the $\{\bar{1}11\}$ form to grow in slices of thickness $d_{\bar{2}22}$, as also demonstrated by van Rosmalen et al.[26] who attributed the F character to this narrower slice as well. This does not markedly affect the anhydrous equilibrium shape of gypsum at 0 K, since the minimum $\gamma$ values determine the morphological importance of every form (see Table 1); however, halving the slice thickness lowers the corresponding slice energy and then the attachment energy increases.[8] Consequently, the existence of this kind of quasi equi-probable $\{\bar{1}11\}$ profiles is important for explaining the anisotropic growth shape of gypsum. The same considerations apply to the multiple profiles and to the $d_{022}$ slice of the {011} form.

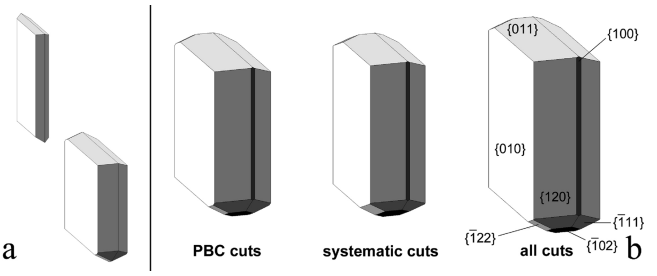


**Figure 8.** Comparison between unrelaxed equilibrium shapes of gypsum: (a) obtained by Simon and Bienfait and by Heijnen and Hartman (from left to right) and (b) in this work.

(b) The alternative PBC $[0\bar{1}1]_b$ (Figure 7c and enlarged view on the right side of Figure 7b) is contained in a slice of thickness $d_{\bar{1}22}$. As already found,[1,2] the [201] PBC running within the same slice is not a true PBC since the end chain energy is repulsive, as it resulted from the calculation of the energy released when an entire building unit ($CaSO_4 \cdot 2H_2O$) deposits at the end of a semi-infinite [201] chain. Since no other PBC can be found within this slice, the $\{\bar{1}22\}$ form has a stepped character.

Finally, it is worth mentioning that another form, the $\{\bar{1}02\}$ pinacoid, potentially could compose the equilibrium shape of gypsum. The thickness of the slice allowed by the space group, $d_{\bar{2}04}$ = 0.154 nm, is too narrow to contain either the $[211]_a$ or the $[211]_b$ PBC (not detailed in Figure 5). Hence the $\{\bar{1}02\}$ form has K character. Nevertheless, two $\{\bar{1}02\}$ profiles can be drawn, one out of them being built by alternating the $[211]_a$ and the $[211]_b$ PBCs.

## 4. The Equilibrium Shape of Gypsum at 0 K

By Wulff's construction,[27] using the minimum $\gamma$ values quoted in Table 1, the different equilibrium shapes of the gypsum crystal were drawn and compared with those obtained by Simon and Bienfait[2] and Heijnen and Hartman[8] (Figures 8 and 9).

Three main considerations can be proposed:

(i) As the potential function describing the bulk crystal field becomes more accurate, the number of forms composing the equilibrium morphology increases. They were three following Simon and Bienfait, that is, {010}, {120}, and $\{0\bar{1}1\}$; then, the $\{\bar{1}11\}$ prism was added by Hartman and Heijnen, while, in this paper, three more forms: $\{\bar{1}22\}$, {100}, and $\{\bar{1}02\}$ make up the equilibrium shape.

(ii) It is worth outlining that not only the equilibrium shape becomes richer in crystallographic forms but also evolves from a strong anisotropy to a fairly good isotropy, especially when the surface relaxation is considered. As a matter of fact, the {010} form, largely dominating the equilibrium shape calculated by Simon and Heijnen, gives way to the {120} prism. This will be particularly

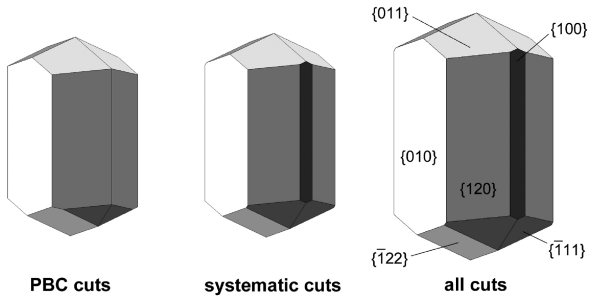


**Figure 9.** The relaxed equilibrium shape of gypsum (this work).

important to correctly evaluate the modification of the equilibrium shape produced by adsorption. Indeed, the {120} surfaces in aqueous solution will be affected by water adsorption much more than the {010} ones, owing to the higher proportion of surface sites, occupied by $Ca^{2+}$ and $SO_4^{2-}$, available for strong solvent interaction.

(iii) In addition to the four singular F forms {010}, {120}, {0$\bar{1}$1}, and {$\bar{1}$11}, two stepped, {100}, {$\bar{1}$22}, and one kinked form, {$\bar{1}$02}, make up the equilibrium shape of gypsum. It is the second time that we show that also nonsingular forms can compose the equilibrium shape of a crystal. Previously, we found that the {0001} form of calcite maintains its intrinsic K character, even after the octopolar reconstruction is carried out to stabilize its surface profile. In that case we showed[11] that the relaxed {0001} profile, reconstructed respecting the surface symmetry imposed by the crystal field of the bulk, gives a $\gamma_{0001}$ value so low to allow the {0001} form to belong to the equilibrium shape of calcite.

## 5. Conclusions

The theoretical equilibrium morphology of gypsum has been reassessed by adopting the semiempirical potential functions proposed by Adam[17] and comparing the values of the athermal specific surface energies ($\gamma_{hkl}$) obtained according to two different methods of choosing the surface configurations of the {*hkl*} forms:

(i) In the Hartman−Perdok method,[8] surface profiles have been drawn respecting the rigorous constraints imposed by the PBC generation and the consequent character found for every {*hkl*} form;

(ii) In the GDIS method,[15] the surface profiles are generated under the only conditions of the electroneutrality and the annihilation of the dipole moment perpendicular to each $d_{hkl}$ slice.

From the relaxed and unrelaxed $\gamma_{hkl}$ values, it follows that the GDIS method usefully integrates the Hartman−Perdok way of predicting surface profiles, by increasing the number of configurations for a given {*hkl*} form; this in turn, is of great value in view of the studies on water adsorption we are going to undertake. Indeed, the adsorption can change the relative stability of the different configurations of the same face and surface profiles favored in a vacuum could not form the most stable interface in the presence of water.

Moreover, the theoretical equilibrium shape of gypsum obtained in this work is substantially modified with respect to those found in the sound papers by Simon and Bienfait[2] and by and Hartman and Heijnen:[5] the traditionally dominant {010} pinacoid is overtaken by the {120} prism and new stepped forms, {100} and {$\bar{1}$22}, along with the kinked {$\bar{1}$02} form, compose the equilibrium shape.

These findings affect the averaged value of the specific surface energy that plays a major role in determining the 3D nucleation frequency of gypsum, whose value is critical especially at temperatures higher than 45 °C where the aqueous solution is more supersaturated with respect to anhydrite than with respect to gypsum so that the former phase should preferentially nucleate, at variance with observations.

These considerations point to the need of critically reconsidering the works on these two minerals and of modeling their interface in aqueous solution by molecular dynamics.

The method we use in this and in a work on the {1*k*0} vicinal forms (in preparation) allows us to determine a richer morphology of gypsum that is an indication of a richer growth morphology. In this work, we cannot give details on the faces in the [001] zone, but we can anticipate that the integration of the two methods revealed that either the morphology obtained by PBC or the other by GDIS is favored, depending on the orientation of the face: this is due to the weight of the relaxation energy highly dependent, for a given face, on the kind of surface reconstruction. The resulting crystal habit is in rather good agreement with the observed natural crystals, in particular those grown close to equilibrium discovered in the Naica mine.

As pointed out in the quoted thesis by Simon, a contact twin can form on a face that is stable. Our syncretic strategy allowed us to recognize that the (100) is a component of the gypsum morphology and that a crystal can grow on it in a faulty orientation. Indeed, using the results here exposed, we have shown that 100 is the composition plane, we have calculated the twinning and the adhesion energy of the (100) contact twin, and we are able to rationalize the frequency of observation of this type of twin; this is the object of a work we are writing.

Summarizing, the method we propose allows us to open new research avenues on the study of the gypsum−water interface, and it is fruitful concerning the ability to explain both the generation mechanisms of the most recurrent {100} contact twins of gypsum and the regular occurrence of the stable and of the erroneously supposed unstable {1*k*0} vicinal forms, in particular in the striking example of the giant crystals from the Naica mine[13] whose growth conditions are quite well-known.

## Appendix I

Parametric ratio, parameters, and space groups of gypsum. The number of $CaSO_4 \cdot 2H_2O$ units is 4 for all the cells described in the following Tables 2−4.

(i) Frames referred to the morphological cell: 0.372: 1: 0.412; $\beta$ = 113.83° (Friedel[33]):(ii) An alternative choice

**Table 2**

| $a_0$ (Å) | $b_0$ (Å) | $c_0$ (Å) | $\beta$ (°) | space group | authors |
|---|---|---|---|---|---|
| 5.63 | 15.15 | 6.23 | 113.83 | *C*2/*c* | De Jong, Bouman[3] |
| 5.67 | 15.201 | 6.274 | 113.91 | *A*2/*a* | Cole, Lancucki[28] |
| 5.678 | 15.213 | 6.286 | 114.08 | *A*2/*a* | Heijnen, Hartman[8] |

($\tau_1'$, $\tau_2'$, $\tau_3'$) has been made, which is related to the morphological cell ($\tau_1$, $\tau_2$, $\tau_3$) as follows: ($\tau_1' = -\tau_3$; $\tau_2' = \tau_2$; $\tau_3' = \tau_1 + \tau_3$).

**Table 3**

| $a_0$ (Å) | $b_0$ (Å) | $c_0$ (Å) | $\beta$ (°) | space group | authors |
|---|---|---|---|---|---|
| 6.28 | 15.15 | 6.51 | 127.40 | *A*2/*a* | Ramdohr, Strunz[29] |
| 6.284 | 15.20 | 6.52 | 127.414 | *C*2/*c* | Boyens, Icharam[30] |

From the transformation of the reference frame, a new angle $\beta' \approx 128°$ generates in between $\tau_1'$ and $\tau_3'$, as it may be seen in Figure 10.

Parameters and space groups of the ($\tau_1'$, $\tau_2'$, $\tau_3'$) cell are as follows:

**Table 4**

| $a_0$ (Å) | $b_0$ (Å) | $c_0$ (Å) | $\beta$ (°) | space group | authors |
|---|---|---|---|---|---|
| 5.67 | 15.15 | 6.51 | 118.38 | *I*2/*a* | Bragg[31] |
| 5.68 | 15.15 | 6.52 | 118.383 | *I*2/*a* | Pake[32] |
| 5.679 | 15.202 | 6.522 | 118.43 | *I*2/*a* | Pedersen, Semmingsen[18] |

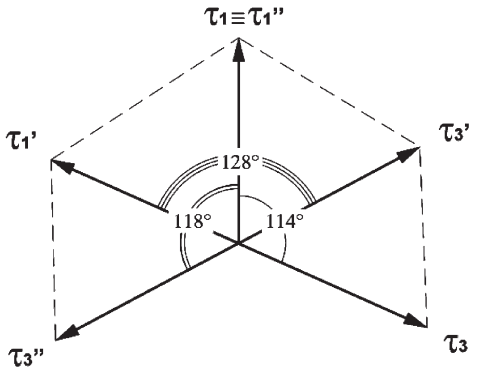


**Figure 10.** Geometrical relationships among the different reference frames of gypsum, according to the description made in the Appendix. The [010] or the [0$\bar{1}$0] direction is perpendicular to the drawing plane.

(iii) Lastly, there is another choice ($\tau_1''$, $\tau_2''$, $\tau_3''$) which is related to the frame ($\tau_1$, $\tau_2$, $\tau_3$) according to the relations: $\tau_1'' = \tau_1$, $\tau_2'' = -\tau_2$, $\tau_3'' = -(\tau_1 + \tau_3)$. In this case, the new angle $\beta' \approx 118°$.

## Appendix II

**Table 5**[a]

| bond | potential function | *A* (erg) | $\rho$ (Å) | *C* (erg Å$^{-6}$) | cut off (Å) |
|---|---|---|---|---|---|
| Ca−O | Buckingham | $2.6454627 \times 10^{-9}$ | 0.29310 | 0 | 20 |
| Ca−$O_{ws}$ | id. | $2.5585221 \times 10^{-9}$ | 0.29213 | 0 | 20 |
| O−$O_{ws}$ | id. | $9.1543406 \times 10^{-8}$ | 0.22425 | $1.2127396 \times 10^{-10}$ | 20 |
| H−O | id. | $3.9749945 \times 10^{-9}$ | 0.05978 | 0 | 20 |
| O−O | id. | $1.65943202 \times 10^{-7}$ | 0.20000 | $4.1539860 \times 10^{-11}$ | 15 |
| H−$O_{ws}$ | id. | $6.3482454 \times 10^{-10}$ | 0.25000 | $1.6020000 \times 10^{-11}$ | 20 |

| bond | type | *k* (erg Å$^{-2}$) | cut off (Å) |
|---|---|---|---|
| $O_{ws}$−$O_{ws}$ | spring | $3.355389 \times 10^{-10}$ | 0.8 |

| bond | type | *D* | $\beta$ (Å$^{-1}$) | $r_0$ (Å) | cut off (Å) |
|---|---|---|---|---|---|
| H−$O_{ws}$ | intra-Morse | $9.9383274 \times 10^{-12}$ | 2.2200 | 0.9240 | 1.1 |
| O−S | id. | $8.0100000 \times 10^{-12}$ | 1.2000 | 1.5050 | 1.8 |

| bond | type | *A* (erg Å$^{12}$) | B (erg Å$^{6}$) | cut off (Å) |
|---|---|---|---|---|
| $O_{ws}$−$O_{ws}$ | Lennard-Jones 12 | $6.3030657 \times 10^{-8}$ | $6.75243 \times 10^{-11}$ | 40.0 |

| bond | type | *K* (erg rad$^{-2}$) | $\theta$ (°) | cut off (Å) |
|---|---|---|---|---|
| O−S−O | harm. | $2.4030000 \times 10^{-11}$ | 109.47° | 1.8 1.8 3.2 |
| H−$O_{wc}$−H | three body id. | $6.7280796 \times 10^{-12}$ | 108.69° | 1.2 1.2 2.4 |

[a] Note: the w, c, and s subscripts indicate water, core and shell, respectively.

## References


(1) Simon, B. Thèse, Université d'Aix-Marseille, **1968**.
(2) Simon, B.; Bienfait, M. *Acta Crystallogr.* **1965**, *19*, 750–756.
(3) De Jong, W. F.; Bouman, J. *Z. Kristallogr.* **1938**, *100*, 275–276.
(4) Weijnen, M. P. C.; van Rosmalen, G. M.; Bennema, P.; Rijpkema, J. J. M. *J. Cryst. Growth* **1987**, *82*, 509–527.
(5) Hartman, P.; Heijnen, W. M. M. *J. Cryst. Growth* **1983**, *63*, 261–264.
(6) Gelius, U.; Roos, B.; Siegbahn, B. *Theor. Chim. Acta* **1971**, *23*, 59–66.
(7) Del Re, G. *J. Chem. Soc.* **1958**, 4031–4040.
(8) Heijnen, W. M. M.; Hartman, P. *J. Cryst. Growth* **1991**, *108*, 290–300.
(9) Van der Voort, E.; Hartman, P. *J. Cryst. Growth* **1991**, *112*, 445–450.
(10) Hartman, P.; Kern, R. *C. R. Acad. Sci. Paris* **1964**, *258*, 4591–4593.
(11) Bruno, M.; Massaro, F. R.; Prencipe, M.; Aquilano, D. *CrystEngComm* in press.
(12) Goldschmidt, V. *Atlas der Kristallformen*; Universitätverlag: Heidelberg, Germany, 1923−1931; Vol. 1−9.
(13) García-Ruiz, J. M.; Villasuso, R.; Ayora, C.; Canals, A.; Otálora, F. *Geology* **2007**, *35* (4), 327–330.
(14) Hartman, P. In *Crystal Growth: An Introduction*; Hartman, P., Eds.; North Holland Publishing Co.: Amsterdam, 1973; pp 367−402.
(15) Fleming, S.; Rohl, A. *Z. Kryst.* **2005**, *220*, 580–584.
(16) Gale, J. D. *J. Chem. Soc. Faraday Trans.* **1997**, *93* (4), 629–637.
(17) Adam, C. D. *J. Solid State Chem.* **2003**, *174*, 141–151.
(18) Pedersen, B. F.; Semmingsen, D. *Acta Crystallogr.* **1982**, *B38*, 1074–1077.
(19) GDIS (the acronym is not given by the authors of the code) is a GTK based program for the display and manipulation of isolated molecules and periodic systems. GTK (GIMP Tool Kit) is a highly usable, feature rich toolkit for creating graphical user interfaces.
(20) A primitive PBC is an uninterrupted periodic chain of strong bonds disregarding the condition of stoichiometry and electroneutrality; a partial PBC is defined as an uninterrupted chain of strong bonds, consisting of one or more primitive PBCs and additional ions as to be neutral; a complete PBC may be constituted by two or more partial PBCs.
(21) Woensdregt, C. F. quoted by 't Hart, J. *Can. Mineralogist* **1978**, *16*, 175–547.
(22) Woensdregt, C. F. *Z. Kristallogr.* **1982**, *161*, 15–33.
(23) Rubbo, M.; Bruno, M.; Prencipe, M. *Cryst. Growth Des.* **2009**, *9*, 404–408.
(24) Bruno, M.; Aquilano, D.; Prencipe, M. *Cryst. Growth Des.* **2009**, *9*, 1912–1916.
(25) Massaro, F. R.; Pastero, L.; Rubbo, M.; Aquilano, D. *J. Cryst. Growth* **2008**, *310*, 706–715.
(26) Van Rosmalen, G. M.; Marchée, W. G. J.; Bennema, P. *J. Cryst. Growth* **1976**, *35*, 169–176.
(27) Kern, R. In *Morphology of Crystals. Part A*; Sunagawa, I., Eds.; Terra Scientific Publishing Co.: Tokyo, 1987; pp 77−206.
(28) Cole, W. E.; Lancucki, C. J. *Acta Crystallogr.* **1974**, *B30*, 921–929.
(29) Ramdohr, P.; Strunz, H. *Klockmann's Lehrbuch der Mineralogie*, 16th ed.; Ferdinand Enke Verlag: Stuttgart, Germany, 1978.
(30) Boyens, J. C. A.; Icharam, V. V. H. *Zeit. Krist.* **2002**, *217*, 9–10.
(31) Bragg, L.; Claringbull, G. F. *Crystal Structure of Minerals*; Bell & Sons: London, 1965.
(32) Pake, G. E. *J. Chem. Phys.* **1948**, *16*, 327–336.
(33) Friedel, G. *Bull. Soc. Franç. Min. Crist.* **1912**, *35*, 45–49.